Experimental Demonstration of Room-Temperature Spin Transport in *n*-Type Germanium Epilayers

S. Dushenko,[1] M. Koike,[1] Y. Ando,[1,2] T. Shinjo,[2] M. Myronov,[3] and M. Shiraishi[1,2,*]
[1]*Graduate School of Engineering Science, Osaka University, Toyonaka 560-8531, Japan*
[2]*Department of Electronic Science and Engineering, Kyoto University, Kyoto 615-8510, Japan*
[3]*Department of Physics, The University of Warwick, Coventry CV47AL, United Kingdom*
(Received 8 September 2014; revised manuscript received 20 April 2015; published 13 May 2015)

We report an experimental demonstration of room-temperature spin transport in *n*-type Ge epilayers grown on a Si(001) substrate. By utilizing spin pumping under ferromagnetic resonance, which inherently endows a spin battery function for semiconductors connected with a ferromagnet, a pure spin current is generated in the *n*-Ge at room temperature. The pure spin current is detected by using the inverse spin-Hall effect of either a Pt or Pd electrode on *n*-Ge. From a theoretical model that includes a geometrical contribution, the spin diffusion length in *n*-Ge at room temperature is estimated to be 660 nm. Moreover, the spin relaxation time decreases with increasing temperature, in agreement with a recently proposed theory of donor-driven spin relaxation in multivalley semiconductors.

DOI: 10.1103/PhysRevLett.114.196602 PACS numbers: 72.25.Dc, 72.25.Mk, 76.50.+g, 85.75.−d

Group IV semiconductors, such as Si and Ge, continue to attract tremendous attention in spintronics due to their suppression of spin relaxation. The crystal inversion symmetry of Si and Ge precludes the spin relaxation of conduction electrons by the Dyakonov-Perel mechanism [1], resulting in a long spin relaxation time. Although the spin-orbit interaction (SOI) of Ge is not negligibly small (0.29 eV), the SOI affects electrons much less than holes in Ge, making *n*-type Ge a promising material for spin transport. Furthermore, compared with Si, Ge possesses a much higher carrier mobility [2]. Thus, it is possible for Ge-based spin transport field effect transistors with small gate lengths to overcome the scaling limits of Si-based devices. Additionally, in recent years, significant success has been achieved in the production of a high-quality GeO_2 layer with a gate function in the *n*-channel Ge-based metal oxide semiconductor field effect transistor [3]. Moreover, spin injection and spin relaxation in Ge have been extensively studied using electron spin resonance [4–9] and optical techniques [10–13]. However, in spite of all the recent progress in the Ge field and in contrast to Si, spin transport in Ge using nonlocal four-terminal techniques has only been observed at low temperatures to date [14–16]. Spin transport has been reported through a Ni/Ge/AlGaAs junction; however, optical spin injection lacks the scalability needed for nanoelectronic applications [17]. Some electrical studies [18–20] reported spin injection into highly doped *n*-Ge at room temperature (RT), raising the possibility that RT Ge spintronics can be realized. Unfortunately, these studies used a three-terminal method, the reliability of which is now being called into question. Many recent studies demonstrated that signals in the three-terminal geometry originate not from spin accumulation in nonmagnetic channels but from magnetic field–dependent tunneling through localized states [21–27]. Other studies revealed that NiFe itself generates electromotive forces by the inverse spin-Hall effect (ISHE) [28] and the planar Hall effect [29]. Careful control experiments are indispensable to eliminate the self-induced electromotive forces from NiFe. Thus, realization of RT spin transport in Ge is still an open challenge, and is long awaited for further progress in semiconductor spintronics. The spin pumping–induced generation of a pure spin current originates from magnetization $\mathbf{M}(t)$ precession in the ferromagnetic layer under ferromagnetic resonance (FMR) conditions [30–33]. Using this highly promising tool, successful spin transport has been achieved at RT in single-layer graphene [34] and in semiconducting conjugated polymers [35]. In our experiment, the magnetic moment is transferred through the interface of the ferromagnet and the adjacent *n*-Ge layer, creating a pure spin current in the latter [Fig. 1(a)]. After propagation through the *n*-Ge channel, the spins are absorbed in the metal electrode with a strong SOI, Me^{SOI} [36–38] (Pt and Pd in our study). The SOI in Me^{SOI} converts the spin current into a charge current via the ISHE [39–43], which is described by the following equation [44]: $\mathbf{J}_C = D_{\mathrm{ISHE}}\mathbf{J}_S \times \boldsymbol{\sigma}$, where D_{ISHE} represents the ISHE efficiency of the material. The generated charge current can be detected as the voltage at the end of the Me^{SOI} strip.

Although the electronic properties of Ge are superior to those of Si, Ge wafers are heavier, less durable, and much more expensive than their Si analogs. Thus, it is desirable to combine the high mobility of Ge channels with the durability and low cost of Si wafers. However, the 4.2% lattice mismatch between Si and Ge precludes the direct epitaxial growth of high-quality relaxed Ge layers on top of Si wafers. Efforts to overcome this difficulty are still

 © 2015 American Physical Society

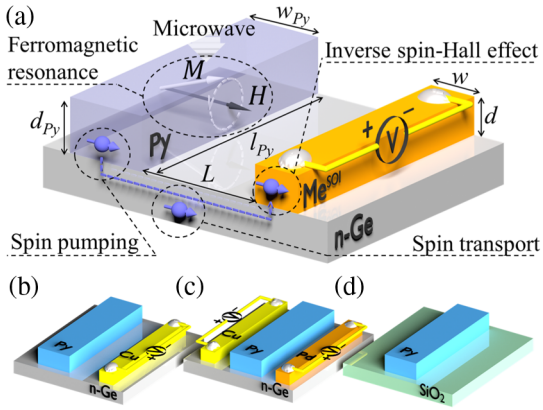

FIG. 1 (color online). A schematic illustration of (a) the spin transport experiment in the Py/n-Ge/Me^{SOI} device, the (b) Py/n-Ge/Cu and (c) Cu/n-Ge/Py/n-Ge/Pd samples used in the control experiments, and the (d) Py/SiO_2 samples used for the spin current density estimation.

ongoing in Ge-related research [45–48]. In our study, high-quality Ge channels were successfully grown on top of Si (001) substrates using a two-temperature method. Additionally, in contrast to the usual use of solid-source molecular beam epitaxy and low-energy plasma-enhanced chemical vapor deposition for the production of high-quality channels, our channel was produced using the reduced pressure-chemical vapor deposition technique that is highly suitable for industrial production. The process described in this study is therefore readily translatable to commercial applications.

Figure 1(a) shows the structure of the n-Ge-based spin transport device used in our study. The Ge epilayers were grown on standard p^--Si(001) substrates using the two-temperature growth method by reduced pressure–chemical vapor deposition [46,48]. The structure consisted of a 1-μm-thick undoped Ge epilayer and a 50 nm heavily n-type doped Ge epilayer with a phosphorous doping concentration of $\sim 1.0 \times 10^{19}$ cm^{-3} and a degree of relaxation of 104%, calculated from the analysis of measured high-resolution x-ray diffraction symmetrical and asymmetrical reciprocal space maps. This overrelaxation of the Ge channel is attributed to the difference in the thermal expansion coefficients between Ge and Si; i.e., the Ge channel is 100% relaxed during the temperature growth, but is under slight tensile strain after cooling down to RT [46,47,49,50]. The Ge epilayers were measured to have a root mean square roughness below 1 nm by atomic force microscopy (AFM) and had a threading dislocation density of $\sim 5 \times 10^6$ cm^{-2}. Me^{SOI} and $Ni_{80}Fe_{20}$ (Py) strips were formed on top of the n-Ge epilayers by electron beam lithography and electron beam evaporation. The samples were etched in a 10% hydrofluoric acid solution and washed in deionized water prior to the evaporation of Me^{SOI} to remove the natural Ge oxide layer. Hereafter, we refer to this sample type as Py/n-Ge/Me^{SOI}. Samples were placed in the center of a TE_{102} cavity inside an electron spin resonance system with a microwave frequency $f = 9.58$ GHz. Ag paste was used to attach one Cu wire at each end of the Me^{SOI} strip to detect the voltage signal. Using identical procedures, three different sample types were prepared, that is, Py/n-Ge/Cu [Fig. 1(b)], Cu/n-Ge/Py/n-Ge/Pd [Fig. 1(c)], and Py/SiO_2 [Fig. 1(d)]. The first two sample types were used for the control experiments, whereas the third was used to calculate the spin current density at the Py/n-Ge interface. Measurements, when not mentioned explicitly, were carried out at RT.

We now proceed to describe the experimental results. Figure 2(a) shows the first derivative of the FMR spectrum, dI/dH. The red and black lines represent the spectra for Py/SiO_2 and Py/n-Ge/Pd, respectively. The enhanced peak-to-peak width of the FMR signal in the second case is due to the presence of spin pumping from Py into n-Ge under FMR conditions. The ISHE voltage is proportional to the generated spin current, the amplitude of which is proportional to the microwave absorption, which is maximized at the resonance field H_{FMR}. Hence, the voltage signal from the ISHE takes the shape of a symmetric peak with respect to H_{FMR}. The detected electromotive force was fitted using the function [44] $V(H) = V_{ISHE}\frac{\Gamma^2}{(H-H_{FMR})^2+\Gamma^2} + V_{asym}\frac{-2\Gamma(H-H_{FMR})}{(H-H_{FMR})^2+\Gamma^2} + aH + b$, where the first term describes the symmetric contribution to the voltage signal from the ISHE. The second term describes the asymmetric contribution to the voltage from different spurious effects, including the anomalous Hall effect, for which the voltage sign is reversed at the resonance field H_{FMR}; additionally, the last two terms represent the offset voltage [Fig. 2(b)]. Fitting the experimentally detected voltage yielded the values of $V_{ISHE} = 1.73$ μV and $V_{asym} = -0.43$ μV. Finally, to eliminate any heating effects, the average of V_{ISHE} for opposing orientations of the external magnetic field $\mathbf{H}$, $\theta_H = 0°$ [shown in Fig. 1(a)] and $\theta_H = 180°$,

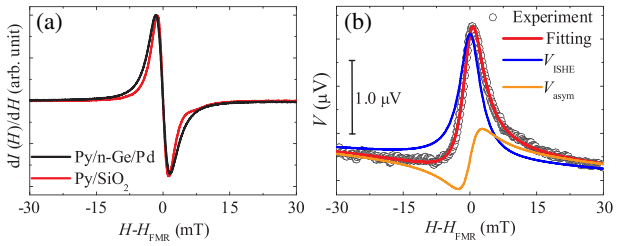

FIG. 2 (color online). (a) FMR signal dI/dH dependence on the in-plane external magnetic field $\mathbf{H}$ for the Py/n-Ge/Pd (black line) and Py/SiO_2 (red line) samples at $\theta_H = 0°$. H_{FMR} and I denote the resonance field and the microwave absorption intensity, respectively. (b) The electromotive force V detected from the Pd strip dependence on the in-plane external magnetic field $\mathbf{H}$ for the Py/n-Ge/Pd sample at $\theta_H = 0°$. Open circles denote the experimental data, and the colored lines show the fitting result.

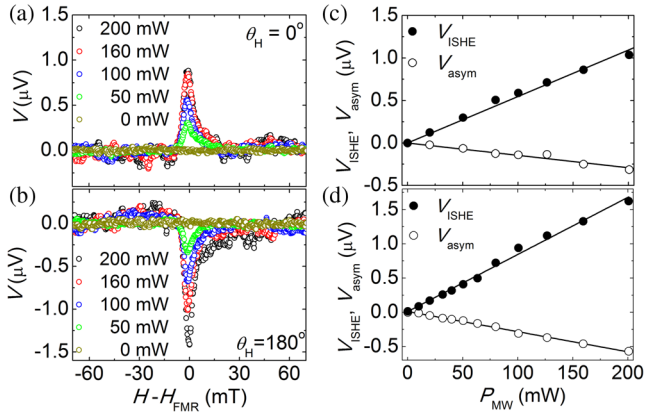

FIG. 3 (color online). The electromotive force V detected at different microwave powers from the Pt strip of the Py/n-Ge/Pt sample under FMR for the two external magnetic field $\mathbf{H}$ orientations (a) $\theta_H = 0°$ and (b) $\theta_H = 180°$. (c),(d) Microwave power dependence of V_{ISHE} (filled circles) and V_{asym} (empty circles) contributions to the electromotive force V detected from the $\mathrm{Me^{SOI}}$ strip of the Py/n-Ge/$\mathrm{Me^{SOI}}$ device, where the solid lines denote the linear fit. (c) $\mathrm{Me^{SOI}} = \mathrm{Pt}$. (d) $\mathrm{Me^{SOI}} = \mathrm{Pd}$.

was calculated as $V_{\mathrm{ISHE}} = (V_{\mathrm{ISHE}}|_{\theta_H=0°} - V_{\mathrm{ISHE}}|_{\theta_H=180°})/2$, giving a value of $V_{\mathrm{ISHE}} = 1.62\ \mu\mathrm{V}$. Figures 3(a)–3(b) show that an analogous symmetrical voltage signal was detected from the Py/n-Ge/Pt sample.

V_{ISHE} is proportional to the square of the microwave magnetic field h, making V_{ISHE} linearly proportional to the microwave (MW) power P_{MW}, as $V_{\mathrm{ISHE}} \propto h^2 \propto P_{\mathrm{MW}}$ [42,51]. Consistent with this prediction, V_{ISHE} increased linearly with P_{MW} for both the Py/n-Ge/Pt and Py/n-Ge/Pd samples [Figs. 3(c)–3(d)]. The reversal of $\mathbf{H}$ to the opposite direction causes $\boldsymbol{\sigma}$ to change sign, which in turn leads to a change in the sign of the ISHE electric field $\mathbf{E}_{\mathrm{ISHE}} \propto \mathbf{J}_C$. Figures 3(a)–3(b) demonstrate the change in sign of the electromotive force upon the reversal of the magnetic field $\mathbf{H}$ to the opposite direction, thus demonstrating that the relation $\mathbf{J}_C = D_{\mathrm{ISHE}}\mathbf{J}_S \times \boldsymbol{\sigma}$ for the ISHE holds in our system.

Next, we theoretically calculated the amplitude of V_{ISHE} for the Py/n-Ge/Pd sample. The estimation of the real part of the mixing conductance $g_r^{\uparrow\downarrow}$ and the spin current density at the ferromagnet-nonferromagnet interface is well established in a number of papers [42,43]. We obtained $g_r^{\uparrow\downarrow} = 2.15 \times 10^{19}\ \mathrm{m^{-2}}$, and the spin current density at the Py/n-Ge interface was $j_S^{\mathrm{Py}/n\text{-Ge}} = 1.33 \times 10^{-9}\ \mathrm{J\,m^{-2}}$ (see the Supplemental Material [52]). Furthermore, we proposed a simple geometrical model to take into account the spin current dissipation in the n-Ge channel. During spin transport from Py to Pd through the n-Ge channel, the density of the spin current $j_S^{\mathrm{Py}/n\text{-Ge}}$ is exponentially damped on the spin diffusion length $\lambda_{n\text{-Ge}}$ of n-Ge. Taking into account our device geometry, we assumed that half of the Py strip contributes to the spin current in the direction of the Pd strip. Integrating over this half gives the spin current density at the n-Ge/Pd interface as

$$j_S^{n\text{-Ge/Pd}} = j_S^{\mathrm{Py}/n\text{-Ge}} \frac{1}{w_{\mathrm{Pd}}} \int_0^{(w_{\mathrm{Py}}/2)} e^{-[(L_{\text{Py-Pd}}+x)/\lambda_{n\text{-Ge}}]} dx$$
$$= j_S^{\mathrm{Py}/n\text{-Ge}} e^{-(L_{\text{Py-Pd}}/\lambda_{n\text{-Ge}})} \frac{\lambda_{n\text{-Ge}}}{w_{\mathrm{Pd}}} (1 - e^{-(w_{\mathrm{Py}}/2\lambda_{n\text{-Ge}})}), \quad (1)$$

where $w_{\mathrm{Pd}} = 1.5\ \mu\mathrm{m}$ is the width of the Pd strip. The gap length $L_{\text{Py-Pd}}$ was measured to be 620 nm using AFM. The conductivity of the Pd strip $\sigma_{\mathrm{Pd}} = 1.97 \times 10^6\ (\Omega\mathrm{m})^{-1}$ [42] is over 1 order of magnitude higher than that of our n-Ge channel $\sigma_{n\text{-Ge}} = 8.22 \times 10^4\ (\Omega\mathrm{m})^{-1}$; this fact and the calculated value of $j_S^{n\text{-Ge/Pd}}$ allowed us to modify the commonly used expression [42], and we finally obtained the voltage of the ISHE from the Pd strip as

$$V_{\mathrm{ISHE}} = \frac{l_{\mathrm{Py}}\theta_{\mathrm{SHE}}\lambda_{\mathrm{Pd}} \tanh(d_{\mathrm{Pd}}/2\lambda_{\mathrm{Pd}})}{d_{\mathrm{Pd}}\sigma_{\mathrm{Pd}}} \left(\frac{2e}{\hbar}\right) j_S^{n\text{-Ge/Pd}}, \quad (2)$$

where $l_{\mathrm{Py}} = 900\ \mu\mathrm{m}$ is the length of the Py strip, $d_{\mathrm{Pd}} = 10$ nm is the thickness of the Pd strip, and $\theta_{\mathrm{SHE}} = 0.01$ [42] and $\lambda_{\mathrm{Pd}} = 9$ nm [54] are the spin-Hall angle and the spin diffusion length of the Pd strip, respectively. By equating Eq. (2) to the experimentally measured $V_{\mathrm{ISHE}} = 1.62\ \mu\mathrm{V}$, we calculated the value of the spin diffusion length in the n-Ge to be $\lambda_{n\text{-Ge}} = 680$ nm. Finally, taking the data from all samples into account, we estimated the spin diffusion length in the n-Ge channel at RT to be $\lambda_{n\text{-Ge}} = 660 \pm 200$ nm. The spin diffusion length in highly doped n-Ge (with a doping concentration of $n = 2 \times 10^{19}\ \mathrm{cm^{-3}}$) was reported to be 580 nm at 4 K [14]. An important step forward was made three years later, when $\lambda_{n\text{-Ge}} = 590$ nm was realized at 150 K in an n-Ge channel ($n = 10^{18}\ \mathrm{cm^{-3}}$) [16]. We now make a final step toward RT Ge spintronics by achieving $\lambda_{n\text{-Ge}} = 660 \pm 200$ nm at RT.

As a part of the control experiment, a sample of Py/n-Ge/Cu was prepared with a Cu strip [Fig. 1(b)], instead of a $\mathrm{Me^{SOI}}$ strip. The gap distance $L_{\text{Py-Cu}}$ was measured to be 490 nm. Figures 4(g) and 4(h) show the detected electromotive force under a microwave excitation of 200 mW for two sample orientations. In contrast to the Py/n-Ge/Pt and Py/n-Ge/Pd samples, the electromotive force possesses an asymmetric shape that reverses its sign over H_{FMR}. This fact strongly indicates that the origin of the symmetric part of the electromotive force signal in the Py/n-Ge/Pt and Py/n-Ge/Pd samples is the ISHE in Pt and Pd, which have a significantly stronger SOI than Cu (the SOI scales approximately as Z^4, where Z is the atomic number of the material [38]). As a second part of the control experiment, the sample of Cu/n-Ge/Py/n-Ge/Pd [Fig. 1(c)] was produced with both Pd and Cu strips, which were located on different sides of the Py strip. The gap

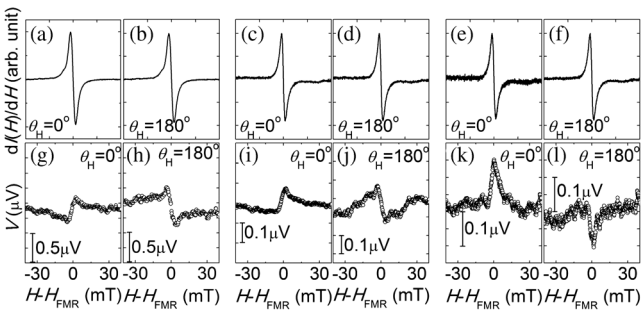

FIG. 4. The FMR signal dI/dH dependence on the in-plane external magnetic field **H** for Py/n-Ge/Cu for (a) $\theta_H = 0°$ and (b) $\theta_H = 180°$, and for Cu/n-Ge/Py/n-Ge/Pd for (c), (e) $\theta_H = 0°$ and (d),(f) $\theta_H = 180°$. The electromotive force V detected under FMR from the Cu strip of the Py/n-Ge/Cu sample (g) for $\theta_H = 0°$ and (h) $\theta_H = 180°$, from the Cu strip of the Cu/n-Ge/Py/n-Ge/Pd sample (i) for $\theta_H = 0°$ and (j) $\theta_H = 180°$, from the Pd strip of the Cu/n-Ge/Py/n-Ge/Pd sample (k) for $\theta_H = 0°$ and (l) $\theta_H = 180°$.

distance between Py and Pd was measured to be $L_{\text{Py-Pd}} = 320$ nm, whereas that between Py and Cu was measured to be $L_{\text{Py-Cu}} = 420$ nm; the microwave power was set to 40 mW. From the Cu strip, similar to the previous case, an asymmetric electromotive force shape was detected [Figs. 4(i) and 4(j)], which is in contrast to the electromotive force from the Pd strip; the latter did not change sign over H_{FMR}, but instead acquired a symmetric shape [Figs. 4(k) and 4(l)], as expected from the ISHE. It should be noted that this result provides direct evidence of successful spin transport in n-Ge at RT because an asymmetric signal was detected from Cu, whereas a distinctly symmetric electromotive force was detected from Pt and Pd.

We measured the temperature dependence of the ISHE voltage in the Py/n-Ge/Pt sample to shed light on the spin relaxation mechanism in our n-Ge epilayers. We assumed the Elliott-Yafet mechanism [55,56] of spin Hall conductivity for Pt, i.e., $\lambda_{\text{Pt}}(T) \propto \sigma_{\text{Pt}}(T)$, and a constant spin Hall conductivity with changing temperature [57–59]. Using the aforementioned assumptions, we extracted $\lambda_{n\text{-Ge}}(T)/\lambda_{n\text{-Ge}}(297\ \text{K})$ from Eq. (2) [Fig. 5(a)]. Furthermore, the temperature dependence of the mobility of the n-Ge channel $\mu_{n\text{-Ge}}$ was determined using maximum-entropy mobility spectrum analysis [60,61]. The mobility in the n-Ge channel changed from $210 \pm 30\ \text{cm}^2\,\text{V}^{-1}\,\text{s}^{-1}$ at RT to $376 \pm 30\ \text{cm}^2\,\text{V}^{-1}\,\text{s}^{-1}$ at 130 K [see Fig. S2 of the Supplemental Material [52] for $\mu_{n\text{-Ge}}(T)$]. The spin relaxation time $\tau_{n\text{-Ge}}$ is related to the spin diffusion length by the equation $\lambda_{n\text{-Ge}} = \sqrt{D\tau_{n\text{-Ge}}}$, where D is the diffusion constant directly proportional to the mobility $\mu_{n\text{-Ge}}$. This allowed us to plot the ratio $\tau_{n\text{-Ge}}(T)/\tau_{n\text{-Ge}}(297\ \text{K})$ as a function of temperature [Fig. 5(b)]. The lowest conduction band in germanium consists of four L valleys, with the center Γ valley located 0.14 eV above it. The spin relaxation time due to intravalley scattering between the lower

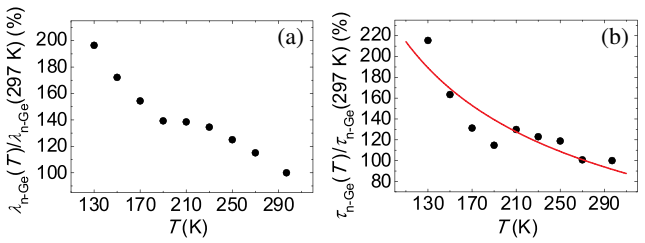

FIG. 5 (color online). Temperature dependence of the (a) spin diffusion length and (b) spin relaxation time of electrons in the n-Ge channel normalized by RT values. The red line is an inverse square root fitting.

conduction and upper valence bands follows a $T^{-7/2}$ dependence [56]. However, due to the spatial inversion and time reversal symmetries of the L point in Ge, the intravalley spin-flip matrix elements for both phonon-induced scattering [62] and impurity-induced scattering [63] are very small. Thus, intravalley-induced spin scattering can only be dominant at low temperatures ($T < 20$ K [62]), rendering intervalley spin scattering as the main spin relaxation mechanism in this work ($T < 130$ K). Recently, a spin relaxation mechanism by intervalley scattering in the presence of a magnetic field originating from g-factor anisotropy was discovered in Ge [64]. However, in our case, due to the degenerate doping and ultrafast spin-conserving momentum relaxation time at temperatures close to RT, this mechanism is suppressed. Using the amplitude of the external magnetic field $B \sim 0.1$ T and an intervalley momentum relaxation time <1 ps [62] in Eq. (4) from Ref. [64], one can find that the contribution to the spin relaxation from the g-factor anisotropy mechanism is negligible compared to intervalley scattering with phonons. Spin relaxation due to intervalley electron-phonon scattering is governed by X phonons, which connect the centers of two different L valleys [13]. These phonons have an energy of approximately 30 meV [13,62,65] and obey the Bose-Einstein temperature distribution. It results in a strong exponential behavior of this spin relaxation time around RT [62]. By contrast, the spin relaxation time showed a weak temperature dependence and increased only by a factor of 2.2 from RT to $T = 130$ K. Therefore, we ruled out intervalley spin relaxation due to phonon scattering as a dominant mechanism in our case. Indeed, we observed saturation of the carrier mobility below 170 K, which indicates the dominance of the ionized impurity over phonon scattering in our highly doped n-Ge channel at least at low temperatures. A recent theory [63] showed that in Ge, impurity scattering spin relaxation is governed by an intervalley short range scattering off the central-cell potential of the impurities. In this theory, in strong degenerate regimes, the spin relaxation time exhibits a $1/\sqrt{T}$ behavior [see Eq. (4) in Ref. [63]], which is similar to the weak dependence of $\tau_{n\text{-Ge}}(T)$ observed in this work. Thus, in our highly doped

n-Ge, impurity spin scattering is dominant over other spin relaxation mechanisms. Finally, in addition to the considered bulk spin relaxation mechanisms, we cannot exclude a possible contribution from interface spin scattering. However, the donor-driven spin relaxation mechanism discussed above holds also for the interface spin relaxation, if the scattering centers at the interface allow for scattering between two valleys residing on different crystallographic axes. From spin transport experiments, the Elliott-Yafet mechanism was reported to be dominant in highly doped *n*-Ge, but the data range was only up to 100 K [14,15], with no correlation of $\tau_{n\text{-Ge}}$ with temperature in the range from 150 to 225 K [16]. Thus, we cover the important range from 130 K to RT and provide experimental evidence for an impurity-driven spin relaxation mechanism in highly doped *n*-Ge.

In summary, we demonstrate spin transport at RT in epitaxial *n*-Ge with a doping concentration of $\sim 1.0 \times 10^{19}$ cm^{-3} using a spin pumping method and the ISHE. The spin diffusion length was estimated to be $\lambda_{n\text{-Ge}} = 660 \pm 200$ nm. The spin relaxation time increased with decreasing temperature, in agreement with a recently proposed theory of donor-driven spin relaxation in multivalley semiconductors [63]. As a result, RT spin transport has now been shown in both pivotal semiconductor materials, Ge and Si, providing new opportunities for the future of semiconductor spintronics.

This research was supported in part by the EPSRC-funded "Spintronic Device Physics in Si/Ge Heterostructures," Grant No. EP/J003263/1, and Platform Grant No. EP/J001074/1. S. D. and M. K. contributed equally to this work.

*Corresponding author.
mshiraishi@kuee.kyoto-u.ac.jp

[1] M. I. Dyakonov and V. I. Perel, Sov. Phys. JETP **33**, 1053 (1971).
[2] S. M. Sze, *Physics of Semiconductor Devices*, 2nd ed. (Wiley-Interscience, New York, 1981).
[3] K. Morii, T. Iwasaki, R. Nakane, M. Takenaka, and S. Takagi, IEEE Electron Device Lett. **31**, 1092 (2010).
[4] G. Feher, D. K. Wilson, and E. A. Gere, Phys. Rev. Lett. **3**, 25 (1959).
[5] D. K. Wilson, Phys. Rev. **134**, A265 (1964).
[6] R. E. Pontinen and T. M. Sanders, Phys. Rev. **152**, 850 (1966).
[7] E. M. Gershenzon, N. M. Pevin, and M. S. Fogelso, Phys. Status Solidi **49**, 411 (1972).
[8] A. I. Veinger, A. G. Zabrodskii, T. V. Tisnek, and S. I. Goloshchapov, Semiconductors **41**, 790 (2007).
[9] A. I. Veinger, A. G. Zabrodskii, T. V. Tisnek, and S. I. Goloshchapov, Semiconductors **42**, 1274 (2008).
[10] C. Hautmann, B. Surrer, and M. Betz, Phys. Rev. B **83**, 161203(R) (2011).
[11] C. Guite and V. Venkataraman, Phys. Rev. Lett. **107**, 166603 (2011).
[12] E. J. Loren, J. Rioux, C. Lange, J. E. Sipe, H. M. van Driel, and A. L. Smirl, Phys. Rev. B **84**, 214307 (2011).
[13] F. Pezzoli, F. Bottegoni, D. Trivedi, F. Ciccacci, A. Giorgioni, P. Li, S. Cecchi, E. Grilli, Y. Song, M. Guzzi, H. Dery, and G. Isella, Phys. Rev. Lett. **108**, 156603 (2012).
[14] Y. Zhou, W. Han, L.-T. Chang, F. Xiu, M. Wang, M. Oehme, I. A. Fischer, J. Schulze, R. K. Kawakami, and K. L. Wang, Phys. Rev. B **84**, 125323 (2011).
[15] L.-T. Chang, W. Han, Y. Zhou, J. Tang, I. A. Fischer, M. Oehme, J. Schulze, R. K. Kawakami, and K. L. Wang, Semicond. Sci. Technol. **28**, 015018 (2013).
[16] K. Kasahara, Y. Fujita, S. Yamada, K. Sawano, M. Miyao, and K. Hamaya, Appl. Phys. Express **7**, 033002 (2014).
[17] C. Shen, T. Trypiniotis, K. Y. Lee, S. N. Holmes, R. Mansell, M. Husain, V. Shah, X. V. Li, H. Kurebayashi, I. Farrer, C. H. de Groot, D. R. Leadley, G. Bell, E. H. C. Parker, T. Whall, D. A. Ritchie, and C. H. W. Barnes, Appl. Phys. Lett. **97**, 162104 (2010).
[18] K. R. Jeon, B. C. Min, Y. H. Jo, H. S. Lee, I. J. Shin, C. Y. Park, S. Y. Park, and S. C. Shin, Phys. Rev. B **84**, 165315 (2011).
[19] A. T. Hanbicki, S.-F. Cheng, R. Goswami, O. M. J. van't Erve, and B. T. Jonker, Solid State Commun. **152**, 244 (2012).
[20] J.-C. Rojas-Sanchez, M. Cubukcu, A. Jain, C. Vergnaud, C. Portemont, C. Ducruet, A. Barski, A. Marty, L. Vila, J.-P. Attane, E. Augendre, G. Desfonds, S. Gambarelli, H. Jaffre, J.-M. George, and M. Jamet, Phys. Rev. B **88**, 064403 (2013).
[21] Y. Aoki, M. Kameno, Y. Ando, E. Shikoh, Y. Suzuki, T. Shinjo, and M. Shiraishi, Phys. Rev. B **86**, 081201(R) (2012).
[22] T. Uemura, K. Kondo, J. Fujisawa, K. Matsuda, and M. Yamamoto, Appl. Phys. Lett. **101**, 132411 (2012).
[23] O. Txoperena, M. Gobbi, A. Bedoya-Pinto, F. Golmar, X. Sun, L. E. Hueso, and F. Casanova, Appl. Phys. Lett. **102**, 192406 (2013).
[24] H. N. Tinkey, P. Li, and I. Appelbaum, Appl. Phys. Lett. **104**, 232410 (2014).
[25] A. G. Swartz, S. Harashima, Y. Xie, D. Lu, B. Kim, C. Bell, Y. Hikita, and H. Y. Hwang, Appl. Phys. Lett. **105**, 032406 (2014).
[26] Y. Song and H. Dery, Phys. Rev. Lett. **113**, 047205 (2014).
[27] O. Txoperena, Y. Song, L. Qing, M. Gobbi, L. E. Hueso, H. Dery, and F. Casanova, Phys. Rev. Lett. **113**, 146601 (2014).
[28] A. Tsukahara, Y. Ando, Y. Kitamura, H. Emoto, E. Shikoh, M. P. Delmo, T. Shinjo, and M. Shiraishi, Phys. Rev. B **89**, 235317 (2014).
[29] L. Chen, S. Ikeda, F. Matsukura, and H. Ohno, Appl. Phys. Express **7**, 013002 (2014).
[30] Y. Tserkovnyak, A. Brataas, and G. E. W. Bauer, Phys. Rev. Lett. **88**, 117601 (2002).
[31] Y. Tserkovnyak, A. Brataas, G. E. W. Bauer, and B. I. Halperin, Rev. Mod. Phys. **77**, 1375 (2005).
[32] A. Brataas, Y. Tserkovnyak, G. E. W. Bauer, and P. J. Kelly, arXiv:1108.0385.
[33] K. Ando, S. Takahashi, J. Ieda, Y. Kajiwara, H. Nakayama, T. Yoshino, K. Harii, Y. Fujikawa, M. Matsuo, S. Maekawa, and E. Saitoh, J. Appl. Phys. **109**, 103913 (2011).

[34] Z. Tang, E. Shikoh, H. Ago, K. Kawahara, Y. Ando, T. Shinjo, and M. Shiraishi, Phys. Rev. B **87**, 140401(R) (2013).
[35] S. Watanabe, K. Ando, K. Kang, S. Mooser, Y. Vaynzof, H. Kurebayashi, E. Saitoh, and H. Sirringhaus, Nat. Phys. **10**, 308 (2014).
[36] T. Tanaka, H. Kontani, M. Naito, T. Naito, D. S. Hirashima, K. Yamada, and J. Inoue, Phys. Rev. B **77**, 165117 (2008).
[37] M. Morota, Y. Niimi, K. Ohnishi, D. H. Wei, T. Tanaka, H. Kontani, T. Kimura, and Y. Otani, Phys. Rev. B **83**, 174405 (2011).
[38] H. L. Wang, C. H. Du, Y. Pu, R. Adur, P. C. Hammel, and F. Y. Yang, Phys. Rev. Lett. **112**, 197201 (2014).
[39] N. S. Averkiev and M. I. Dyakonov, Sov. Phys. Semicond. **17**, 393 (1983).
[40] A. A. Bakun, B. P. Zakharchenya, A. A. Rogachev, M. N. Tkachuk, and V. G. Fleisher, JETP Lett. **40**, 1293 (1984).
[41] S. O. Valenzuela and M. Tinkham, Nature (London) **442**, 176 (2006).
[42] K. Ando and E. Saitoh, J. Appl. Phys. **108**, 113925 (2010).
[43] O. Mosendz, V. Vlaminck, J. E. Pearson, F. Y. Fradin, G. E. W. Bauer, S. D. Bader, and A. Hoffmann, Phys. Rev. B **82**, 214403 (2010).
[44] E. Saitoh, M. Ueda, H. Miyajima, and G. Tatara, Appl. Phys. Lett. **88**, 182509 (2006).
[45] D. Choi, Y. Ge, J. S. Harris, J. Cagnon, and S. Stemmer, J. Cryst. Growth **310**, 4273 (2008).
[46] V. A. Shah, A. Dobbie, M. Myronov, and D. R. Leadley, Thin Solid Films **519**, 7911 (2011).
[47] Y. Yamamoto, P. Zaumseil, T. Arguirov, M. Kittler, and B. Tillack, Solid State Electron. **60**, 2 (2011).
[48] V. H. Nguyen, A. Dobbie, M. Myronov, and D. R. Leadley, J. Appl. Phys. **114**, 154306 (2013).
[49] Y. Ishikawa, K. Wada, D. D. Cannon, J. Liu, H.-C. Luan, and L. C. Kimerling, Appl. Phys. Lett. **82**, 2044 (2003).
[50] J. M. Hartmann, A. Abbadie, A. M. Papon, P. Holliger, G. Rolland, T. Billon, J. M. Fedeli, M. Rouviere, L. Vivien, and S. Laval, J. Appl. Phys. **95**, 5905 (2004).
[51] K. Ando, S. Takahashi, J. Ieda, H. Kurebayashi, T. Trypiniotis, C. H. W. Barnes, S. Maekawa, and E. Saitoh, Nat. Mater. **10**, 655 (2011).
[52] See Supplemental Material at http://link.aps.org/supplemental/10.1103/PhysRevLett.114.196602, which includes Ref. [53], for the calculation of the mixing conductance $g_r^{\uparrow\downarrow}$ and the spin current density $j_S^{\mathrm{Py}/n\text{-}\mathrm{Ge}}$.
[53] C. Kittel, Phys. Rev. **73**, 155 (1948).
[54] J. Foros, G. Woltersdorf, B. Heinrich, and A. Brataas, J. Appl. Phys. **97**, 10A714 (2005).
[55] R. J. Elliott, Phys. Rev. **96**, 266 (1954).
[56] Y. Yafet, in *Solid State Physics 14*, edited by F. Seitz and D. Turnbull (Academic, New York, 1963), p. 1.
[57] L. Vila, T. Kimura, and Y. C. Otani, Phys. Rev. Lett. **99**, 226604 (2007).
[58] S. R. Marmion, M. Ali, M. McLaren, D. A. Williams, and B. J. Hickey, Phys. Rev. B **89**, 220404(R) (2014).
[59] R. Ohshima, H. Emoto, T. Shinjo, Y. Ando, and M. Shiraishi, J. Appl. Phys. **117**, 17D136 (2015).
[60] W. A. Beck and J. R. Anderson, J. Appl. Phys. **62**, 541 (1987).
[61] S. Kiatgamolchai, M. Myronov, O. A. Mironov, V. G. Kantser, E. H. C. Parker, and T. E. Whall, Phys. Rev. E **66**, 036705 (2002).
[62] P. Li, Y. Song, and H. Dery, Phys. Rev. B **86**, 085202 (2012).
[63] Y. Song, O. Chalaev, and H. Dery, Phys. Rev. Lett. **113**, 167201 (2014).
[64] P. Li, J. Li, L. Qing, H. Dery, and I. Appelbaum, Phys. Rev. Lett. **111**, 257204 (2013).
[65] J.-M. Tang, B. T. Collins, and M. E. Flatte, Phys. Rev. B **85**, 045202 (2012).